Received: 2 April 2019 | Revised: 24 June 2019 | Accepted: 9 July 2019

DOI: 10.1002/term.2938

Check for updates

RESEARCH ARTICLE

WILEY

Composite clinoptilolite/PCL-PEG-PCL scaffolds for bone regeneration: In vitro and in vivo evaluation

Ahmet Engin Pazarçeviren[1] | Tayfun Dikmen[2] | Korhan Altunbaş[2] | Volkan Yaprakçı[3] | Özge Erdemli[4] | Dilek Keskin[1,5] | Ayşen Tezcaner[1,5]

[1] Department of Engineering Sciences, Middle East Technical University, Ankara, Turkey

[2] Department of Histology and Embryology, Afyon Kocatepe University, Afyon, Turkey

[3] Department of Surgery, Afyon Kocatepe University, Afyon, Turkey

[4] Department of Molecular Biology and Genetics, Başkent University, Ankara, Turkey

[5] Center of Excellence in Biomaterials and Tissue Engineering, Middle East Technical University, Ankara, Turkey

Correspondence
Prof. Dr. Ayşen Tezcaner, Department of Engineering Sciences, Middle East Technical University, Ankara, Turkey.
Email: tezcaner@metu.edu.tr

Funding information
METU Scientific Research Coordination Unit, Grant/Award Number: BAP-03-10-2016-003

Abstract

In this study, clinoptilolite (CLN) was employed as a reinforcement in a polymer-based composite scaffold in bone tissue engineering and evaluated in vivo for the first time. Highly porous, mechanically stable, and osteogenic CLN/PCL-PEG-PCL (CLN/PCEC) scaffolds were fabricated with modified particulate leaching/compression molding technique with varying CLN contents. We hypothesized that CLN reinforcement in a composite scaffold will improve bone regeneration and promote repair. Therefore, the scaffolds were analyzed for compressive strength, biodegradation, biocompatibility, and induction of osteogenic differentiation in vitro. CLN inclusion in PC-10 (10% w/w) and PC-20 (20% w/w) scaffolds revealed 54.7% and 53.4% porosity, higher dry (0.62 and 0.76 MPa), and wet (0.37 and 0.45 MPa) compressive strength, greater cellular adhesion, alkaline phosphatase activity (2.20 and 2.82 mg/g_{DNA}/min), and intracellular calcium concentration (122.44 and 243.24 g Ca/mg_{DNA}). The scaffolds were evaluated in a unicortical bone defect at anterior aspect of proximal tibia of adult rabbits 4 and 8 weeks postimplantation. Similar to in vitro results, CLN-containing scaffolds led to efficient regeneration of bone in a dose-dependent manner. PC-20 demonstrated highest quality of bone union, cortex development, and bone-scaffold interaction at the defect site. Therefore, higher CLN content in PC-20 permitted robust remodeling whereas pure PCEC (PC-0) scaffolds displayed fibrous tissue formation. Consequently, CLN was proven to be a potent reinforcement in terms of promoting mechanical, physical, and biological properties of polymer-based scaffolds in a more economical, easy-to-handle, and reproducible approach.

KEYWORDS

bone union, clinoptilolite, cortex development, PCL-PEG-PCL, zeolite, press-fit scaffold

1 | INTRODUCTION

Intensive research in tissue engineering field has provided various processing techniques means and materials to produce bone tissue scaffolds. Combination of polymers and nanoclays in composite scaffolds allows the fabrication of tailor-made scaffolds with extensive interconnected pores and surface properties that permit cellular adhesion, migration, and tissue ingrowth (Ambre, Katti, & Katti, 2013; Cao et al., 2015). These scaffolds can also be designed to possess good mechanical strength to accommodate compression from surrounding bone and to provide easier handling during the surgical operation (Zhai et al., 2017).

Among the biocompatible synthetic polymers, poly-ε-caprolactone (PCL) appears as the most utilized polymer (Bañobre-López et al., 2011; Dash & Konkimalla, 2012). PCL is a semicrystalline

 © 2019 John Wiley & Sons, Ltd.

thermoplastic polyester having low glass transition (~−60°C) and moderate melting point (~60°C). Therefore, it has been used as the polymer in composite scaffolds for various tissue engineering applications to grant mechanical stability at 37°C (Correa, Carmona, Simão, Capparelli Mattoso, & Marconcini, 2017; Kai et al., 2016). The degradation process may take a long time despite the fact that PCL may undergo hydrolytic cleavage (Dziadek, Pawlik, Menaszek, Stodolak-Zych, & Cholewa-Kowalska, 2015). For this reason, PCL can be modified with bioresorbable hydrophilic polymer polyethylene glycol (PEG) to improve degradation kinetics by increasing the amount of interacting water molecules per chain (Nagasaki, 2011). Accordingly, copolymers of PCL and PEG can be utilized for scaffolding to promote faster biodegradation while preserving mechanical strength of the overall structure (Stanković et al., 2014; Wang et al., 2017).

Nanoclays have been used to enhance mechanical, chemical, and biological properties of the thermoplastic polymers (Gaharwar et al., 2014; Marras, Kladi, Tsivintzelis, Zuburtikudis, & Panayiotou, 2008). One of the naturally occurring nanoclays is clinoptilolite (CLN; $(KNa_2Ca_2(Si_{28}Al_7)O_{72}{\cdot}24H_2O)$). It is a mesoporous aluminosilicate, which can coordinate mono- and divalent metal ions such as sodium, potassium, magnesium, and calcium (Rožić et al., 2005). Furthermore, it has been successfully used as a feed supplement in animal husbandry and fertilizer in agriculture (Eroglu, Emekci, & Athanassiou, 2017; Polat, Karaca, Demir, & Onus, 2004). In addition, we previously reported that inclusion of CLN can improve mechanical (compressive strength and modulus) and chemical properties (serum protein adsorption) of scaffolds and enhance osteogenic differentiation of stem cells in vitro without inclusion of any other osteogenic factor (Pazarçeviren, Erdemli, Keskin, & Tezcaner, 2017).

In this study, we hypothesized that CLN can act as a cost-effective reinforcement in a polymer-based bone tissue scaffold promoting faster regeneration. Additionally, CLN/PCEC scaffolds were fabricated and tested in vivo environment for the first time. Mechanically stable, highly porous and 3D CLN/PCEC scaffolds were prepared with modified particulate leaching/compression molding technique. The scaffolds were analyzed for compressive strength, biodegradation, biocompatibility, and osteogenic differentiation prior to in vivo analysis. Then, scaffolds were evaluated in a unicortical bone defect at anterior aspect of proximal tibia of adult rabbits. To test our hypothesis, histological analyses were conducted at fourth and eighth weeks postimplantation to determine the rate of bone union, cortex development, and interaction between scaffold and bone.

2 | MATERIALS AND METHODS

2.1 | Materials

ε-caprolactone, PEG (M_n = 4,000 Da), lipase from porcine pancreas, ethanol (absolute), Triton X-100, sodium ethylenediamine tetraacetic acid (EDTA), para-nitrophenyl phosphate, para-nitrophenol, magnesium chloride hexahydrate, β-glycerphosphate, L-ascorbic acid, Trishydroxyamino methane, o-cresopthalein complexone, 8-hydroxyquinone-5-sulfonic acid, 2-amino-2-methyl-1,3-propanediol, paraformaldehyde, and dexamethasone were purchased from Sigma-Aldrich (Missouri, USA). Dulbecco's Modified Eagle's Medium/F-12, fetal bovine serum, penicillin-streptomycin were obtained from Biowest (Texas, USA) and Alamar Blue, protease inhibitor cocktail and Hoechst 33258 DNA staining reagent from Invitrogen (California, USA). CLN was kindly provided by Rota Mining Corporation (İstanbul, Turkey). The components of Movat's pentachrome staining were all reagent grade.

2.2 | Scaffold preparation

Composite scaffolds were prepared with PCEC and CLN by modified particulate leaching/compression molding technique. Briefly, PCEC (ε-CL:PEG in 24:1 w/w) was synthesized through ring opening polymerization of ε-caprolactone monomer and PEG initiator (PEG, M_n = 4,000 Da) using dibutyltin dilaurate as catalyst under 140°C with continuous N_2 gas flow. CLN (d[50] = 7.5 μm) was used after being decontaminated in acetone for 2 hr and dried under vacuum. After that, PCEC, CLN, and sodium chloride were blended in absolute ethanol to obtain a homogenous slurry. Then, the blend was dried in vacuum and compressed under 250 MPa to 5 × 2 mm (diameter × length) cylindrical composite. Finally, the composites were placed in distilled water at 37°C for 3 days for NaCl leaching to obtain highly porous PCEC/CLN scaffolds. In order to reach homogenous porosity in the final structure, NaCl porogen was ball milled for 40 min at 20 s according to preliminary optimization and passed through a metal mesh to obtain a particle size between 180 and 210 μm. The scaffolds were prepared in predetermined ratios of components as given in Table 1. It is important to note that density of the components play an important role in determination of individual weight of components. For this reason, an equation was devised to calculate final weights of components where density values of PCEC, NaCl, and CLN discs prepared by compression at 250 MPa were found as 1.20, 2.15, and 2.00 g/cm^3, respectively (Equation 1):

$$\frac{m_{NaCl}}{m_{PCEC}+m_{CLN}} = \frac{\rho_{PCEC}{}^{*}x\% + \rho_{CLN}{}^{*}(100-x)\%}{\rho_{NaCl}} * \frac{y}{100-y}. \quad (1)$$

2.3 | Morphological and porosity analysis

Composite scaffolds were photographed using a conventional camera after dripping 50 μl methylene blue (0.1% w/v in distilled water; Figure 1) on top to determine interconnectivity within the structure. Porosity of the scaffolds (n = 6) was determined in absolute ethanol (nonsolvent) by using Equation (2) given below:

TABLE 1 Scaffold groups and weights of components in preparation of scaffolds with a target porosity of 50%

Scaffold annotation	PCEC (mg)	CLN (mg)	NaCl (mg)
PC-0	100	-	180
PC-10	90	10	180
PC-20	80	20	180

Abbreviation: CLN, clinoptilolite.

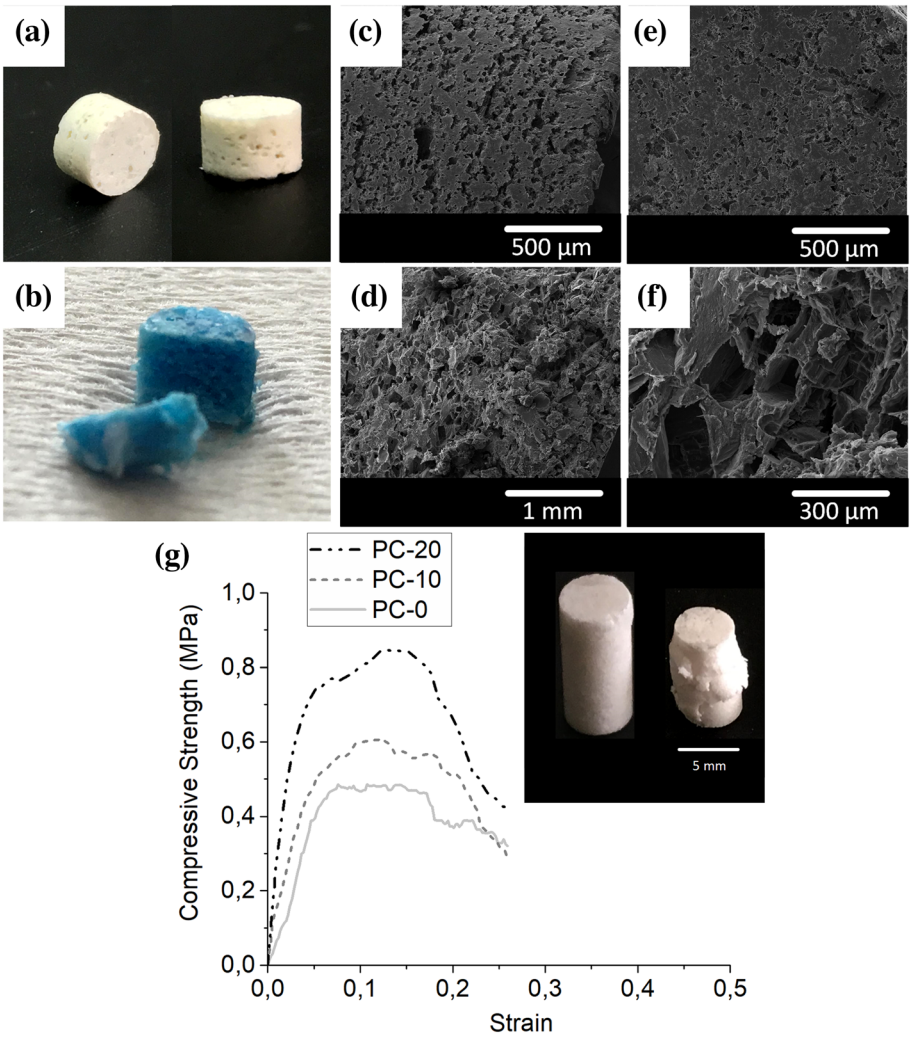

FIGURE 1 Scaffolds after salt leaching (a), and after being stained with methylene blue to observe porosity (b), scanning electron microscopy (SEM) images of side surface (c), cross-section (d), surface (e), and closer view of cross-sections of PC-20 scaffold (f), and wet compressive properties of representative scaffolds from each group, and image of wet PC-20 scaffold before and after compressive analysis is presented as an inset [Colour figure can be viewed at wileyonlinelibrary.com]

$$\textit{Open porosity}\ (\%) = \frac{\textit{Total volume of scaffold} - \textit{residual volume}}{\textit{Volume of ethanol in pores} - \textit{residual volume}} * 100\%. \quad (2)$$

Surface and cross-sectional electrographs were taken using scanning electron microscopy (SEM) and the overall elemental content of the scaffolds was determined with energy dispersive X-ray spectroscopy (EDX, JEOL JSM-6335F FEG/SEM equipped with analytical EDX attachment, Japan).

2.4 | Mechanical analysis

Mechanical properties of the scaffolds were determined through compression analysis. The composite scaffolds were with an aspect ratio of 2/1 to ascertain compressive properties such as compressive strength and modulus. They were soaked in phosphate-buffered saline (PBS) at 37°C overnight and were compressed at 1 mm/min uniaxially up to 25% compressive strain (n = 4; Univert Cellscale, Canada).

2.5 | Biodegradation analysis

Biodegradation analysis was used to study the loss of structural integrity and mechanical properties of scaffolds (n = 4) in time in an environment mimicking in vivo conditions. Prior to analysis, scaffolds were sterilized in 70% (v/v) ethanol-distilled water and UV irradiation for 1 hr. Biodegradation analysis was conducted by incubating scaffolds (n = 3) in a lipase solution (110 U/L in PBS) for various time points (0, 3, 5, 7, 14, 21, and 28 days). At the end of each incubation period, the scaffolds were rinsed, dried, weighed, and change in weight against the initial weight was recorded as percent weight loss. Lipase solution was refreshed daily.

2.6 | In vitro study

As a preliminary study to in vivo analysis, cytocompatibility of the composite scaffolds was tested in vitro. Briefly, the UV sterilized composite scaffolds were seeded with human fetal osteoblast cell line

(hFOB, Passage 4) at a density of 25,000 cells per scaffold for cellular attachment, proliferation, and osteogenic differentiation analyses.

2.6.1 | Cellular attachment and proliferation analyses

hFOB seeded scaffolds (10,000 cells per scaffold, $n = 6$) were placed in tissue culture plates and incubated for 1, 4, and 7 days in 500-µl growth medium (composed of Dulbecco's MEM/F-12 nutrient medium, 10% (v/v) fetal bovine serum, and 1% (v/v) penicillin-streptomycin) at 37°C in carbon dioxide incubator (Panasonic, Japan). At the end of each incubation period, scaffolds were rinsed with PBS, placed in new well plates, and cellular viability analysis by Alamar Blue reagent was conducted according to supplier's protocol (Invitrogen, USA). Relative cellular viability of hFOB on scaffolds was calculated as percent cellular viability where cell viability on pure PCEC scaffolds was taken as 100%. Furthermore, a randomly selected scaffold from each group was thoroughly rinsed with PBS, fixed in 4% (w/v) paraformaldehyde and dehydrated in diluted ethanol series in distilled water (50% to absolute) at the end of Day 1. These samples were examined by SEM to observe the morphology of the cells attached on the samples.

2.6.2 | Osteogenic differentiation analysis

In order to study osteogenic response of the hFOB on scaffolds, hFOB seeded scaffolds (10,000 cells per scaffold, $n = 5$) were cultured in osteogenic media (growth medium containing 10-mM β-glycerphosphate, 50-µg/ml ascorbic acid and 10^{-8} M dexamethasone) for 2 weeks. After incubation of predetermined time periods (2 weeks), scaffolds were rinsed with PBS and placed into cell lysis buffer (1% Triton X-100 containing 200 times diluted protease inhibitor cocktail (Thermo Fisher, USA) and 50-mM sodium EDTA). Aliquots from cell lysates were taken for determining the total DNA amount, alkaline phosphatase activity, and intracellular calcium (ICa) concentration of cells. Cell-free scaffolds of each group ($n = 2$) incubated in osteogenic media were used as negative control.

DNA quantitation

DNA amounts in cell lysates were determined using Hoechst 33258. Initially, aliquots from cell lysates (250 µl) and 5,000 times diluted Hoechst 33258 DNA staining reagent (1,750 µl) in TE buffer (100-mM sodium chloride, 10-mM Trishydroxyamino methane, and 1-mM EDTA at pH 9.00) were mixed (25°C, 5 min). Then, fluorescence of the obtained solutions was measured using a fluoremeter (Turner Biosystems, USA). DNA amounts were determined in cell lysates were determined using the calibration curve constructed with different concentrations of calf thymus DNA in cell lysis buffer (0–250 ng/ml)

Alkaline phosphatase activity of cells

Alkaline phosphatase activity of cells on the scaffolds was determined by determining cellular ALP activity per cellular DNA. An aliquot from each sample was reacted with para-nitrophenyl phosphate solution (supplemented with 10-mM magnesium chloride in distilled water) at 37°C for 1 hr. At the end of reaction, optical density at 405 nm measured. The concentration of the product, para-nitrophenol, was determined using the calibration curve constructed with different concentrations of para-nitrophenol in lysis buffer (0–1,000 µg/ml).

ICa concentration of cells

ICa concentration of the cells on the scaffolds was ascertained employing o-cresophthalein complexone assay as conducted elsewhere (Türkkan et al., 2017). Aliquots from cell lysate samples were combined with o-cresopthalein complexone, 8-hydroxyquinone-5-sulfonic acid, and 2-amino-2-methyl-1,3-propanediol 1:1:2 (v/v/v) solutions, and their optical densities at 560 nm were determined. Calibration curve constructed with known concentrations of calcium chloride in distilled water was used to determine the amounts of ICa of cells on the scaffolds.

2.7 | In vivo study

2.7.1 | Surgical procedure and postoperative observation

New Zealand white rabbits (3–3.5 kg, adult female) were maintained in a room with controlled temperature (approximately 22°C) and under 12-hr light/dark cycle kept at the Animal Care Facility of Afyon Kocatepe University Experimental Research Centre. The approval has been received from Afyon Kocatepe University Institutional Animal Ethics Committee (AKUHADYEK-515-15). A total of 24 ($n = 4$ for each scaffold and time period of analysis) rabbits were anesthesized with an intramuscular injection of 2% (w/v) Alfazyne (5 mg/kg Xylazine hydrochloride) and 10% (w/v) Alfamine (25 mg/kg Ketamine hydrochloride). At the proximal tibia of each rabbit, muscles and periosteum were dissected. With a microelectric drill, unicortical anterior tibial defect of a 5 mm radius was opened and washed with sterile PBS continuously to discard debris and prevent thermal necrosis (Figure 3a,b). Finally, implants (5 mm diameter × 2 mm thickness) were press-fitted. Rabbits were placed in standard cages, allowed to access water and food ad libitum. At the end of fourth week and eighth week, rabbits were euthanized with overdose Ketamine hydrochloride, and tibiae with the implants were harvested.

2.7.2 | Evaluation of defect healing

Preparation of samples

Harvested tibiae samples were placed in natural buffered 10% formaldehyde (v/v) solution for 1 day and then put into EDTA decalcification solution for 21 days. Subsequently, samples were dehydrated through graded ethanol series in water and cleared by xylol. Finally, samples were embedded in paraffin and 5-µm sections were placed on poly-L-lysine treated cover slips (VWR, Belgium) for histological analysis.

Histological analysis

Paraffin sections were stained with Movat's pentachrome stain (saffron was replaced with tartrazine): Nuclei are stained in black, fibrous

tissues (FTs) in turquoise, cartilage in blue, newly forming bone in pink–red and mineralized bone in yellow–brown. Histological assessments were made according to Table S1. Quality of union was evaluated in terms of formation of fibrous, fibrocartilaginous, and bony tissue in and around the scaffolds. Cortex development was determined through new bone formation, and bone-scaffold incorporation was scaled according to the properties of interphase between newly forming bone and biodegradable scaffold.

2.8 | Statistical analysis

Data were analyzed by one-way analysis of variance with Tukey's post hoc test for multiple comparisons using SPSS software (ver. 23.0; IBM Corporation, New York, USA). Differences were considered significant at $p < .05$. The histological scores given for each group at the end of analysis were analyzed with nonparametric Mann–Whitney *U* test (Gibson-Corley, Olivier, & Meyerholz, 2013). Data are given as average ± standard deviation.

3 | RESULTS AND DISCUSSION

3.1 | In vitro studies

PCEC-based composite scaffolds were previously fabricated by our group with various compositions using nonsolvent blended compression molding technique (Pazarçeviren et al., 2017). Compared with our previous study, porogen leaching method was optimized to provide better surface porosity with higher surface and cross-sectional pore size for improved cellular invasion and colonization. Therefore, in this study, a predetermined NaCl size distribution was selected, and density-based target porosity was calculated as aforementioned. Then, the scaffolds were prepared by modified particulate leaching/compression molding technique, and they were designed to possess 50% porosity with macropores and microporous channels to conserve mechanical strength in vivo (Figure 1). Additionally, implant press-fitting requires a stiff material to fit in the defected area. Therefore, moderate porosity plays a vital role in manageable implantation, protection of overall scaffold macrostructure, and primary fixation of scaffold, which improves implant success (Knecht et al., 2007). Furthermore, scaffolds were shown to maintain interconnective structure as observed in micropore openings in the pore walls (Figure 1).

Composite scaffolds were intended to possess 50% porosity, and final 3D and interconnective porous scaffolds were obtained at 55%, 54.7%, and 53.4% porosities for PC-0, PC-10, and PC-20, respectively (Table S2). During salt leaching step, leaching of loosely interlocked components could have resulted in higher porosity (>50%). Moreover, increment in weight ratio of CLN led to nonsignificant decrease in porosity (Table 1). It can be speculated that CLN reinforcement might improve compaction owing to plasticizing effect of mineral particles during molding process thus lower porosity was achieved (Khan, Islam, & Khan, 2012).

Scaffolds were incubated in lipase solution in favor of accelerated hydrolytic degradation. Lipase is an esterase present in human blood serum in the range of 30–190 U/L (Azevedo & Reis, 2005). Scaffolds displayed a slow rate of weight loss (max. 3.7 ± 0.8% for PC-20 in 28 days) in lipase solution (110 U/L). Significantly higher weight loss was observed for PC-20 having greater CLN content than PC-0 (Table S2). This suggests that the plasticizing effect of CLN on PCEC chains might have resulted in further bulk degradation due to increased water resorption and thus movement of polymer chains (Salmasi, Nayyer, Seifalian, & Blunn, 2016).

During mechanical analysis, all scaffolds bulged in the middle and started consolidation (Figure 1g). Because stiff materials are expected to display a similar phenomenon, it can be stated that 3D composite porous scaffolds were proven to maintain mechanical strength after salt leaching process (Thadavirul, Pavasant, & Supaphol, 2014). In addition, presence of CLN was shown to reinforce compressive strength (UTS) and modulus (CM) and imparting stiffness (Table S3). It can be stated that increasing the weight ratio of the CLN (d_{CLN} = 2.00 g/cm^3) by sacrificing the volume of PCEC (d_{PCEC} = 1.20 g/cm^3) permitted CLN particles to assume larger volume in PC-20 scaffolds thus providing better compressive characteristics. Montmorillonite (MNT), an aluminosilicate clay, is one of the highly utilized clays in bone tissue engineering field (BTE) as a nanoreinforcement, which improves mechanical properties significantly (Guo et al., 2019). In a study by Torres, Fombuena, Valles-Lluch, and Ellingham (2017), a PCL-based composite scaffold was prepared with halloysite (HS) and hydroxyapatite (HAp). It was observed that starting from 2.5% HS to 7.5% HS presence without altering HAp concentration in the scaffold improved elastic modulus steadily (Torres et al., 2017). In another study, Villaca et al. (2017) combined MNT with chitosan to produce a composite guided bone regeneration membrane. They determined that tensile strength of the membranes reached to 15.2 ± 3.5 MPa, which was higher than that of pure chitosan (9.5 ± 1.5 MPa). Again, it was observed that clays could be introduced to improve mechanical properties of membranes and scaffold which are prepared for BTE (Villaca et al., 2017).

UTS and CM significantly decreased after enzymatic degradation although a small weight loss was obtained after degradation study (Table S2). Enzymatic cleavage of PCEC by lipase might have induced bulk degradation by which polymer chains were broken without an immense weight loss. Compressive stress caused propagation of chain movement due to decrease in ester bonding after degradation, which led to declined UTS and CM (Bawolin, Li, Chen, & Zhang, 2010). Díaz, Sandonis, and Valle (2014) fabricated nanoHAp (nHA)/PCL scaffold and observed higher mechanical strength and higher weight loss with nHA/PCL scaffolds than pure PCL counterparts (Díaz et al., 2014). Another similar finding was observed by Chern, Yang, Shen, and Hung (2013) with their PCL-based microHA, nHA, and alumina (Al_2O_3) reinforced scaffolds. As observed in our study, Chern et al. reported that the presence of inorganic reinforcements increases porosity while exceptionally improving mechanical and biodegradation properties. Consequently, CLN/PCEC composite scaffolds could be pointed out as a 3D composite scaffold structure with good mechanical and physicochemical properties.

Proliferation study revealed that all scaffolds were biocompatible and permitting cellular proliferation because a significant increase in dye reduction was observed from first to seventh day (Figure 2a). SEM analysis was performed to observe overall morphology of hFOB after 1-day incubation on scaffold. It was observed that cells preferred anchoring adjacent to CLN particles detected by EDX analysis (Figures 2d and 3e). This finding was further affirmed by the fact that CLN increment in the scaffolds, such as PC-20 with highest CLN amount, generated a better synthetic environment for hFOB to attach and grow (Figure 2a). In a similar study, Prabha et al. (2019) fabricated a laponite (LPN) clay containing PCL scaffolds having high porosity via solvent casting and lyophilization (Prabha et al., 2019). At the end of 7 days of incubation, they observed that cells increased in number at around 1.5 fold of initial seeded number. Interestingly, in our study, CLN was shown to induce cellular proliferation enabling almost 1.5 fold increase after 1 week of incubation (Figure 2a).

Scaffolds were further analyzed to determine their osteoinductive properties. For this purpose, scaffolds were seeded with hFOB cells, and osteogenic differentiation of hFOB cells was studied by determining ALP activity and ICa concentration. ALP activity of hFOB cells on

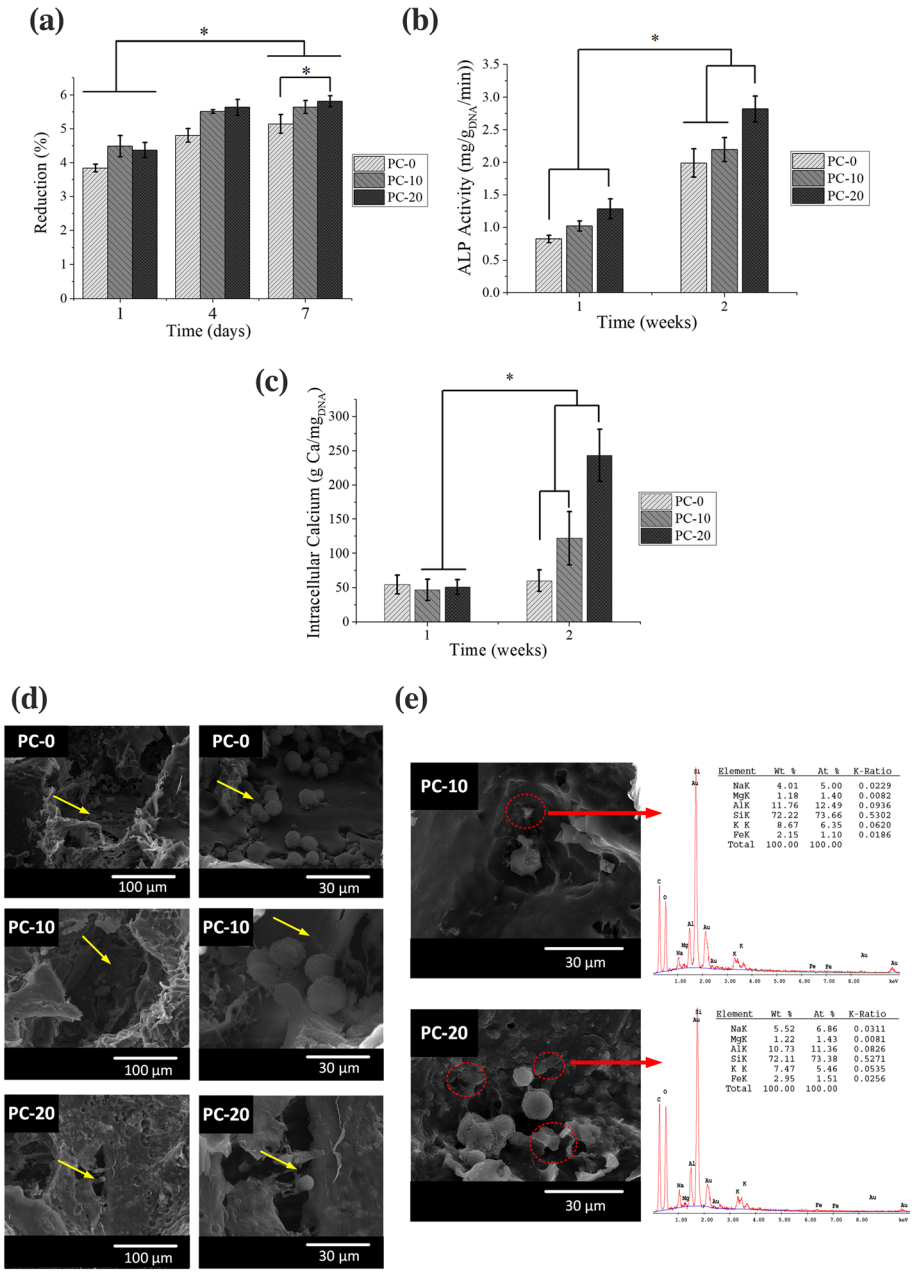

FIGURE 2 In vitro analysis for viability of cells on scaffolds during 7 days of incubation in growth media (a), ALP activity (b), intracellular calcium concentration (C) of human fetal osteoblast (hFOB) cells on scaffolds that were incubated in osteogenic differentiation media for 2 weeks. Cellular attachment on the scaffolds at the end of first day (d) and presence of cells around clinoptilolite (CLN), particles which were detected by energy dispersive X-ray spectroscopy (EDX; e), were shown (yellow arrows show the attached cells, red circles and arrows show the locations of CLN particles.) [Colour figure can be viewed at wileyonlinelibrary.com]

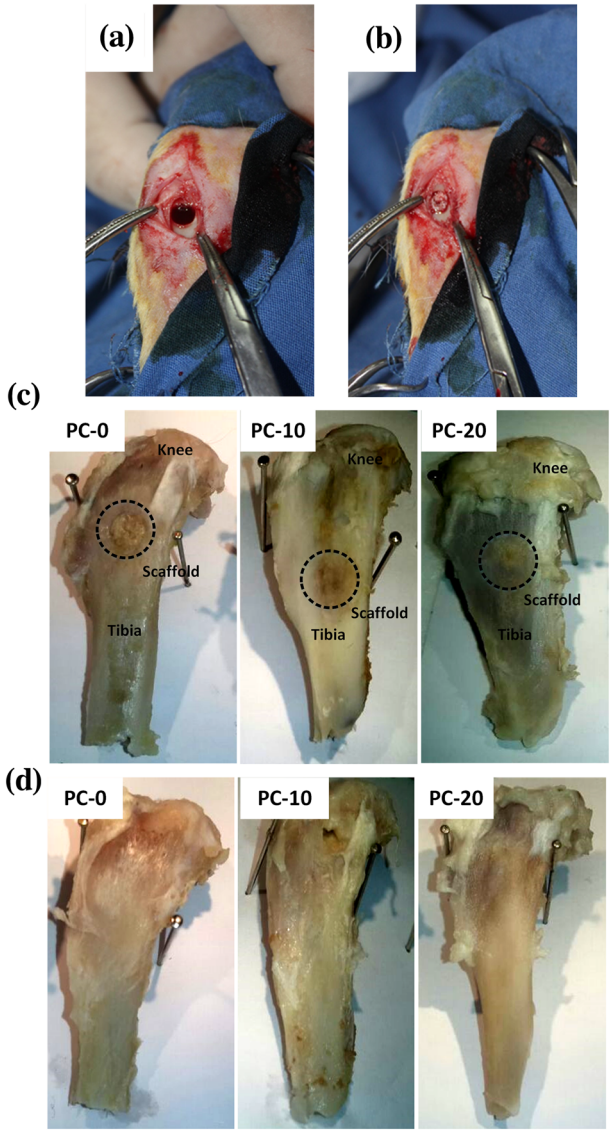

FIGURE 3 Overview of unicortical tibial defect formed (a), after implantation of a scaffold from PC-20 group (b), tibia harvested at the end of fourth week (c) and at the end of eighth week (d) after implantation [Colour figure can be viewed at wileyonlinelibrary.com]

all scaffolds peaked at the second week (Figure 2b). Cells seeded on PC-20 scaffolds displayed the highest ALP activity ($p < .05$) and showed the lowest activity on PC-0 scaffolds without CLN (Figure 2 b). ICa increase followed a similar trend with ALP activity results. ALP activity leads to orthophosphate production and cells tend to store calcium prior to mineralization (Othman, Mustafa, Loon, & Noor, 2016). Osteogenic commitment of hFOB was observed as an increase in ALP and ICa amounts (Figure 2). Significantly higher ICa was observed in CLN containing PC-10 and PC-20 scaffolds. The crosstalk between mechanical stimuli and biochemical cues has been studied intensively. In a study by Sun et al. (2018), it was reported that increment in substrate mechanical strength could upregulate osteogenic lineage markers such as ALP. Through a similar method employed in our study, Demir (2018) prepared zinc-montmorillonite (Zn-MNT)-PCL composite scaffolds by solvent casting/particulate leaching technique (Demir, 2018). A decrease in porosity and an increase in compressive strength were observed when Zn-MNT was introduced. Additionally, it was shown that MNT only (no Zn-MNT) could itself trigger an increase in ALP activity of cells. Therefore, in our study, it is thought that the increase in mechanical strength endowed by the presence of CLN might have led to enhancement of ALP activity and ICa. In addition, CLN as a natural CLN can carry divalent metal ions, especially calcium and readily involve in ion exchange with monovalent ions (Bacakova, Vandrovcova, Kopova, & Jirka, 2018). Consequently, CLN could provide a local increase in calcium ions that might induce osteogenic differentiation (Akmammedov, Huysal, Isik, & Senel, 2018). All in all, it can be stressed that physical (porosity and pore size), mechanical (compressive strength), and chemical (ion make-up and ion release) properties could manifest a combinatorial effect on both cellular growth and cellular proliferation. In this study, it was displayed that CLN could improve previously mentioned properties and can be utilized as a reinforcement in BTE applications.

3.2 | In vivo studies

In vivo performance of the CLN/PCEC scaffolds was investigated by implanting scaffolds in unicortical tibial defect model in rabbits. The study was designed as a brief study that involved evaluation of the bone formation at the defect site at fourth and eighth weeks postimplantation (Figures 1d and 3c). Proximal tibia was selected for forming a 5-mm diameter unicortical defect because this area had been reported as a slow healing and remodeling zone (Gómez-Barrena et al., 2015).

Initial observations on the harvested tibia at the end of fourth weeks of scaffold implantation revealed that PC-0 did not prompt healing as efficiently as PC-10 and PC-20 scaffolds (Figure 5a). Moreover, CLN containing scaffolds accomplished an early closure in defect zone despite the fact that it was superficial to some extend compared with tibia obtained at the end of eighth week (Figure 5b). It is thought that the implant bed and the quality of tissue at defect site play crucial roles in bone healing in addition to biocompatibility and design of implants (Parithimarkalaignan & Padmanabhan, 2013). A healthy and intact host bone around the defect area can trigger bone healing very rapidly owing to presence of osteoblast niche and readily diffusible blood (Keramaris, Calori, Nikolaou, Schemitsch, & Giannoudis, 2008). As a result, a complete recovery on the defect area can be seen for all scaffolds at the end of the study (Figure 5b). However, histological analyses affirmed that although bone growth was observed for PC-0, bone ingrowth and fusion were not achieved (Figure 5a,b). Extensive FT growth in and around the PC-0 scaffolds was observed (Figure 5a). Moreover, PC-0 showed incorporation with the FT and fibroblasts (black arrows, Figure 5b).

Moreover, PC-0 showed a limited area of soft callus formation and immature bone union with hard callus formation (Han, Bhavsar, Leppik, Oliveira, & Barker, 2018). At the end of the study, this group also displayed nonunion with the newly formed spongy bone (SB) through FT. Specifically, incorporation zone at the end of eighth week revealed a thick FT layer (showed in yellow rectangle) as an intermediary in between PC-0 and formed SB (Figure 6a). The closer

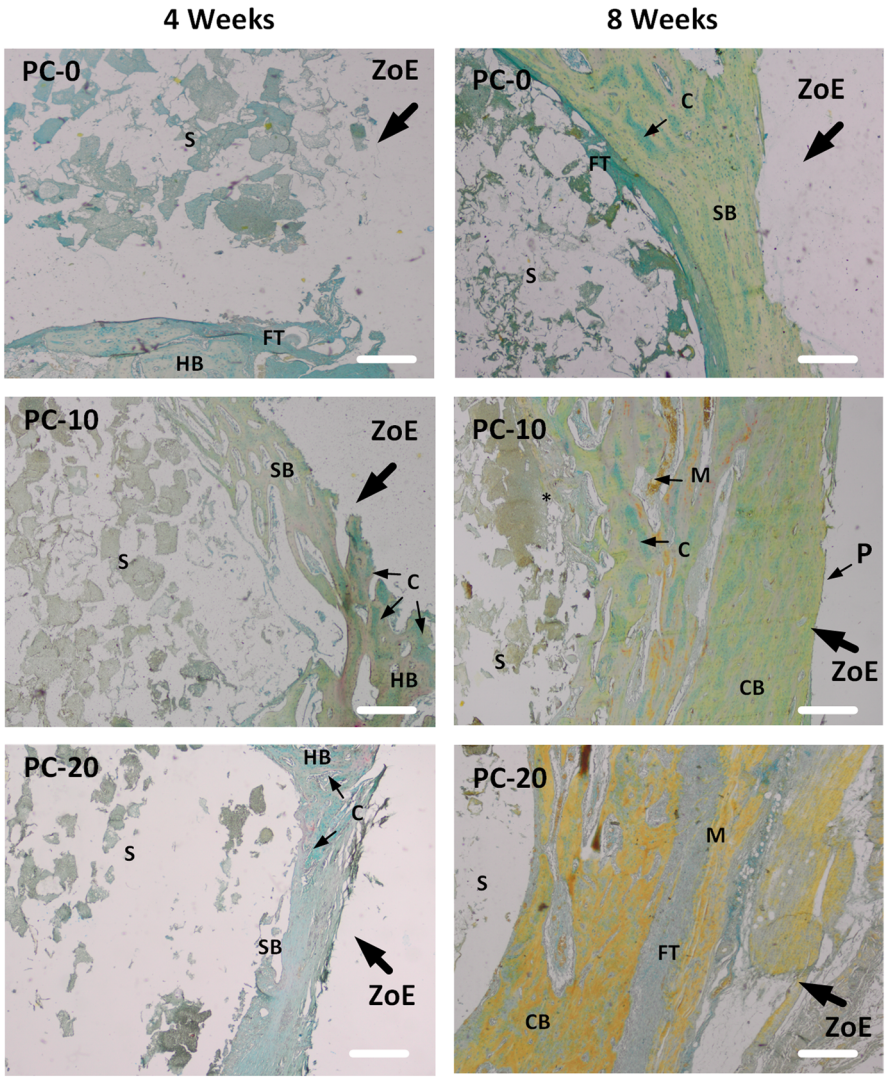

FIGURE 4 Gross observations for Movat's pentachrome staining of sections obtained from the defect site after 4 and 8 weeks postimplantation (C: Cartilagenous tissue, CB: Compact bone, FT: Fibrous tissue, HB: Host bone, M: Mineralized tissue, P: Periosteum, S: Scaffold, SB: Spongy bone, ZoE: Zone of entry). The bar scale is 50 μm [Colour figure can be viewed at wileyonlinelibrary.com]

TABLE 2 Histological scores of each scaffold of PC-0, PC-10, and PC-20 are given (average as avg. and sample standard deviation as St.Dev)

Scaffold	Quality of union (1–5)	Cortex development (1–5)	Bone–scaffold interaction (1–5)
PC-0 at fourth	2	1	1
PC-0 at fourth	1	2	1
PC-0 at fourth	2	1	1
PC-0 at fourth	1	1	1
Avg. ± St.Dev	1.5 ± 0.58	1.25 ± 0.50	1
PC-10 at fourth	2	2	1
PC-10 at fourth	3	2	2
PC-10 at fourth	2	1	1
PC-10 at fourth	2	2	1
Avg. ± St.Dev	2.25 ± 0.5	1.75 ± 0.5	1.25 ± 0.5
PC-20 at fourth	3	1	2
PC-20 at fourth	3	2	1
PC-20 at fourth	3	3	2

(Continues)

TABLE 2 (Continued)

Scaffold	Quality of union (1–5)	Cortex development (1–5)	Bone–scaffold interaction (1–5)
PC-20 at fourth	2	2	2
Avg. ± St.Dev	2.75 ± 0.5	2 ± 0.82	1.75 ± 0.5
PC-0 at eighth	2	2	1
PC-0 at eighth	2	2	1
PC-0 at eighth	3	1	1
PC-0 at eighth	2	3	2
Avg. ± St.Dev	2.25 ± 0.5	2 ± 0.82	1.25 ± 0.5
PC-10 at eighth	2	2	2
PC-10 at eighth	3	3	2
PC-10 at eighth	4	2	3
PC-10 at eighth	4	4	3
Avg. ± St.Dev	3.25 ± 0.96	2.75 ± 0.96	2.5 ± 0.56
PC-20 at eighth	4	3	3
PC-20 at eighth	4	4	3
PC-20 at eighth	5	3	3
PC-20 at eighth	4	4	2
Avg. ± St.Dev	4.25 ± 0.5	3.5 ± 0.58	2.75 ± 0.5

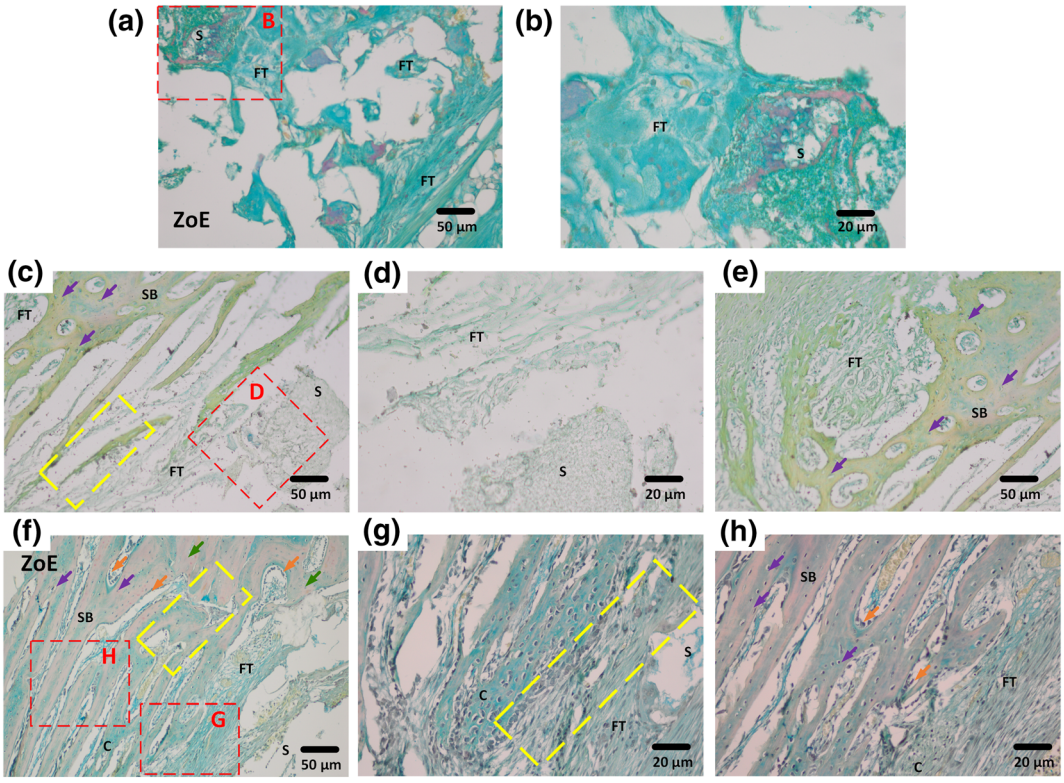

FIGURE 5 Detailed images of Movat's pentachrome staining results at the end of fourth week postimplantation for PC-0 (a, b), PC-10 (c, d, e), and PC-20 (f, g, h). Abbreviations: S: Scaffold, FT: Fibrous tissue, SB: Spongy bone, ZoE: Zone of entry, green arrow: New bone formation, purple arrow: Lacunae, orange arrow: Osteoblast lining, yellow rectangle: Incorporation zone and red rectangle: Closer view of the area of interest [Colour figure can be viewed at wileyonlinelibrary.com]

observation of incorporation zone showed recently grown SB with lacunae (Figure 6c, purple arrows). Moreover, new bone in pinkish color could be observed (Figure 6d). However, a complete healing or cortex formation was only detected in a limited number of PC-0 scaffolds at the end of the in vivo analysis (Figure 6).

After fourth week postimplantation, PC-10 samples exhibited SB formation with presence of hypertrophic cartilage (Clarkin & Olsen, 2010). Consequently, it can be stressed that bone healing at the defect area had started earlier than 4 weeks, and most of the healing steps were successfully undergone without interruption (Figures 4 and 5c). Still, PC-10 showed an interphase with FT growth in and around scaffolds (Figure 5d). When further focused in incorporation zones, less FT and SB formation with fresh lacunae can be observed (Figure 5e). At the end of eighth week, further decrease in size of FT was observed (Figure 6e), and it was replaced with mineralized tissue along with cartilage as an intermediate phase (Figure 6e,f), and a fully constituted periosteum was formed (Figure 6g).

Similar to PC-10, PC-20 implanted host bone showed a fast healing and covered the zone of entry at the end of fourth week (Figure 4). PC-20 showed formation of cartilage as early as fourth week postimplantation, as an initial step of ossification (Figure 5f). Further, it triggered integration to the native bone and developing cortex (Figure 5g). This situation could be a result of effective primary contact with blood in the defect zone (Figure 3). The initial clot formation, which is brought about by blood contact, leads to formation of cytokine gradient allowing attachment molecules to adhere on the surface of construct to both induce cellular attachment and formation of specialized FT, namely, collagenous matrix (Patel et al., 2018). Moreover, presence of SB and declining FT demonstrated the starting of complete healing stage (Figure 5h). Therefore, PC-20 scaffolds showed integration with the newly formed cortex and a thin FT (Figure 6h). In addition, growth of bone through mineralized cartilage within the scaffolds was also observed (Figure 6i,j). Furthermore, according to nonparametric Mann–Whitney *U* test, PC-20 scaffolds were significantly different at both fourth and eighth than PC-0 for all three categories. However, there was no statistically significant difference observed between PC-10 and PC-20 in both time points except for bone-scaffold interaction. PC-20 appeared superior to other groups (Table 2).

Clay-polymer composite scaffolds are one of the highly studied area in BTE. However, there are few studies evaluating clays and their composite scaffolds in vivo. Here, we studied CLN/PCEC scaffolds in a unicortical tibial defect model, and CLN was shown to induce bone regeneration in vivo for the first time (histological scores can be seen in Table S1). In a similar study by Baker, Maerz, Saad, Shaheen, and Kannan (2015), MNT was studied in a poly(D-lactic acid)-based composite scaffold for bone regeneration capacity (Baker et al., 2015). Although MNT was shown to support bone growth, it

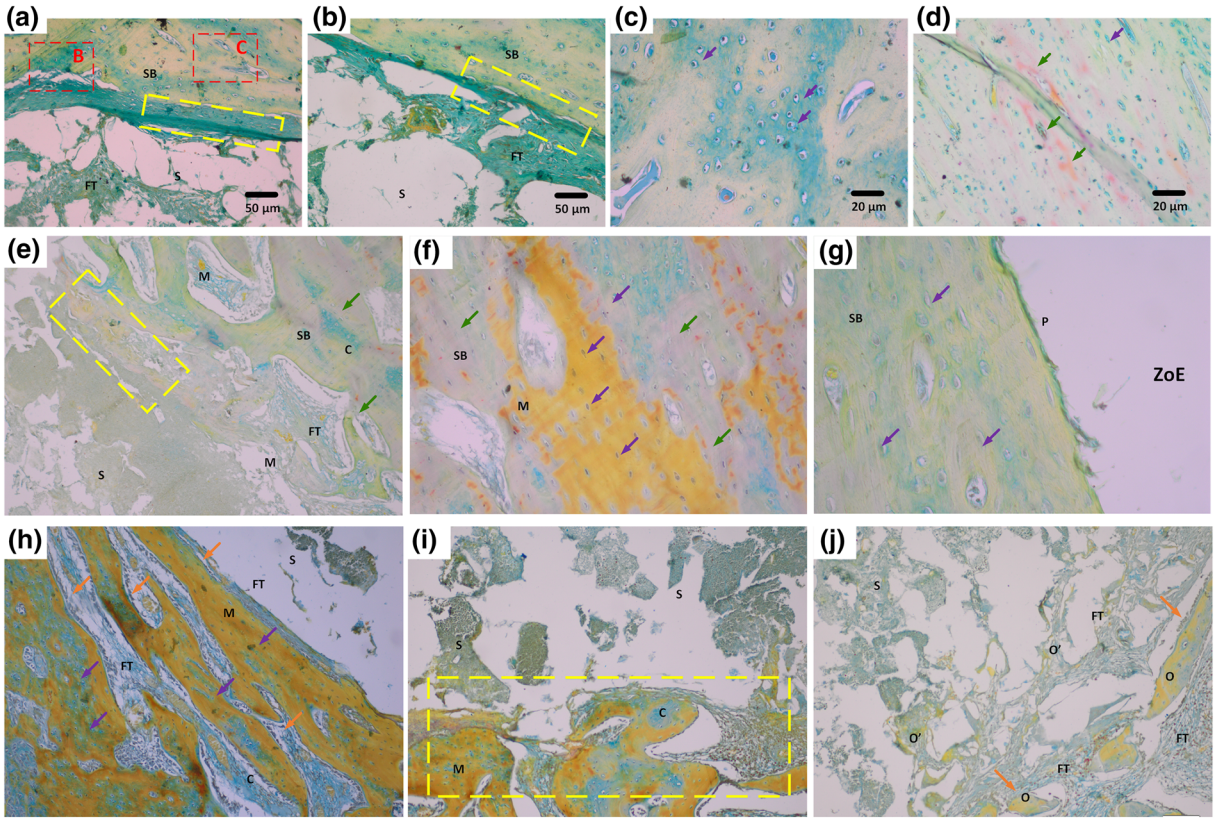

FIGURE 6 Detailed images of Movat's pentachrome staining results at the end of eighth week postimplantation for PC-0 (A-D), PC-10 (E-G), and PC-20 (H-J). Abbreviations: S: Scaffold, FT: Fibrous tissue, SB: Spongy bone, ZoE: Zone of entry, green arrow: New bone formation, purple arrow: Lacunae, orange arrow: Osteoblast lining, yellow rectangle: Incorporation zone and red rectangle: Closer view of the area of interest [Colour figure can be viewed at wileyonlinelibrary.com]

was observed that growth factor and/or HA presence was required to achieve osteogenesis. Zhai et al. (2017) applied LPN, a smectite silicate, in a composite scaffold with poly(*N*-acryloyl glycinamide) (PNAGA) in a rat tibial defect model (Zhai et al., 2017). They used 20% LPN/PNAGA scaffolds in vivo and observed that thicker new bone formation at the periphery of the LPN/PNAGA than blank scaffolds. However, no further analyses were made. In our study, we clearly observed complete cortex and bridging with a surrounding host connective tissue in both PC-10 and PC-20 (Figure 4). Moreover, cortex area was replaced with mineralized collagen matrix evolving into healthy bone structure, especially in PC-20. In addition, presence of cartilage fragments within mineralized tissue points out the samples were in last stage of the bone healing, which is remodeling (Panteli, Pountos, Jones, & Giannoudis, 2015). Additionally, we observed the formation of osteoid pockets in the PC-20 by which it was evidently shown that CLN has high osteogenic and therapeutic potential for BTE (Table 2).

4 | CONCLUSION

This study demonstrates the first work in osteogenic characterization of CLN in a polymer-based composite scaffold in vivo. We focused on employing CLN as a reinforcement to fabricate cost-effective, rapid, and easy-to-handle BTE scaffolds. Here, CLN presence provided an overall enhancement in the highly anticipated properties such as mechanical, physical, and biological properties of the polymer-based scaffolds in vitro. Compressive strength was improved with the inclusion of CLN in scaffolds. In addition, biochemical and biological properties such as cell attachment and maturation substantiated the effectiveness of CLN as an osteogenic reinforcement in vitro. Improvement of osteogenic potential of the scaffolds was in direct correlation with the concentration of CLN within composite scaffolds. Amelioration of bioactivity was also demonstrated in in vivo study. Specifically, PC-20 scaffolds implanted in unicortical tibial defect of rabbits resulted in the formation of completely bridged cortex while remodeling of the bone occurred. Moreover, PC-20 demonstrated greatest quality of bone union, cortex development, and bone-scaffold interaction at the defect site. As a result, higher CLN content in PC-20 permitted bone remodeling whereas pure PCEC (PC-0) scaffolds displayed FT formation. Therefore, osteogenic potential of CLN was successfully shown in vivo as a functional part of PCEC-based scaffold and can be employed in BTE applications.

ACKNOWLEDGEMENT

The authors would like to acknowledge financial support from METU Scientific Research Coordination Unit (project BAP-03-10-2016-003).

CONFLICT OF INTEREST

The authors have declared that there is no conflict of interest.

ORCID

Ayşen Tezcaner https://orcid.org/0000-0003-4292-5856

REFERENCES

Akmammedov, R., Huysal, M., Isik, S., & Senel, M. (2018). Preparation and characterization of novel chitosan/zeolite scaffolds for bone tissue engineering applications. *International Journal of Polymeric Materials and Polymeric Biomaterials*, *67*(2), 110–118.

Ambre, A. H., Katti, D. R., & Katti, K. S. (2013). Nanoclays mediate stem cell differentiation and mineralized ECM formation on biopolymer scaffolds. *Journal of Biomedical Materials Research Part A*, *101*(9), 2644–2660. https://doi.org/10.1002/jbm.a.34561

Azevedo, H. S., & Reis, R. L. (2005). Understanding the enzymatic degradation of biodegradable polymers and strategies to control their degradation rate. In *Biodegradable Systems In Tissue Engineering And Regenerative Medicine* (pp. 177–201). Boca Raton, FL: CRC Press, Taylor & Francis Group.

Bacakova, L., Vandrovcova, M., Kopova, I., & Jirka, I. (2018). Applications of zeolites in biotechnology and medicine - a review. *Biomaterials Science*, *6*(5), 974–989. https://doi.org/10.1039/C8BM00028J

Baker, K. C., Maerz, T., Saad, H., Shaheen, P., & Kannan, R. M. (2015). In vivo bone formation by and inflammatory response to resorbable polymer-nanoclay constructs. *Nanomedicine: Nanotechnology, Biology and Medicine*, *11*(8), 1871–1881.

Bañobre-López, M., Pineiro-Redondo, Y., De Santis, R., Gloria, A., Ambrosio, L., Tampieri, A., … Rivas, J. (2011). Poly (caprolactone) based magnetic scaffolds for bone tissue engineering. *Journal of Applied Physics*, *109*(7), 07B313. https://doi.org/10.1063/1.3561149, https://doi.org/10.1063/1.3561149

Bawolin, N. K., Li, M. G., Chen, X. B., & Zhang, W. J. (2010). Modeling material-degradation-induced elastic property of tissue engineering scaffolds. *Journal of Biomechanical Engineering*, *132*(11), 111001-111001-111007). https://doi.org/10.1115/1.4002551

Cao, X., Wang, J., Liu, M., Chen, Y., Cao, Y., & Yu, X. (2015). Chitosan-collagen/organomontmorillonite scaffold for bone tissue engineering. *Frontiers of Materials Science*, *9*(4), 405–412. https://doi.org/10.1007/s11706-015-0317-5

Chern, M.-J., Yang, L.-Y., Shen, Y.-K., & Hung, J.-H. (2013). 3D scaffold with PCL combined biomedical ceramic materials for bone tissue regeneration. *International Journal of Precision Engineering and Manufacturing*, *14*(12), 2201–2207.

Clarkin, C., & Olsen, B. R. (2010). On bone-forming cells and blood vessels in bone development. *Cell Metabolism*, *12*(4), 314–316.

Correa, A. C., Carmona, V. B., Simão, J. A., Capparelli Mattoso, L. H., & Marconcini, J. M. (2017). Biodegradable blends of urea plasticized thermoplastic starch (UTPS) and poly(ε-caprolactone) (PCL): Morphological, rheological, thermal and mechanical properties. *Carbohydrate Polymers*, *167*, 177–184. https://doi.org/10.1016/j.carbpol.2017.03.051

Dash, T. K., & Konkimalla, V. B. (2012). Poly-ϵ-caprolactone based formulations for drug delivery and tissue engineering: A review. *Journal of Controlled Release*, *158*(1), 15–33. https://doi.org/10.1016/j.jconrel.2011.09.064

Demir, A. K. (2018). Development and characterization of zinc-incorporated montmorillonite/poly (epsilon-caprolactone) composite scaffold for osteogenic tissue-engineering applications. *Polymer Composites*, *39*, E601–E608.

Díaz, E., Sandonis, I., & Valle, M. B. (2014). In vitro degradation of poly (caprolactone)/nHA composites. *Journal of Nanomaterials*, *2014*, 185.

Dziadek, M., Pawlik, J., Menaszek, E., Stodolak-Zych, E., & Cholewa-Kowalska, K. (2015). Effect of the preparation methods on architecture, crystallinity, hydrolytic degradation, bioactivity, and biocompatibility of PCL/bioglass composite scaffolds. *Journal of Biomedical Materials Research Part B: Applied Biomaterials*, *103*(8), 1580–1593.

Eroglu, N., Emekci, M., & Athanassiou, C. G. (2017). Applications of natural zeolites on agriculture and food production. *Journal of the Science of Food and Agriculture*, *97*, 3487–3499. https://doi.org/10.1002/jsfa.8312

Gaharwar, A. K., Mukundan, S., Karaca, E., Dolatshahi-Pirouz, A., Patel, A., Rangarajan, K., … Khademhosseini, A. (2014). Nanoclay-enriched poly (ε-caprolactone) electrospun scaffolds for osteogenic differentiation of human mesenchymal stem cells. *Tissue Engineering Part A*, *20*(15-16), 2088–2101.

Gibson-Corley, K. N., Olivier, A. K., & Meyerholz, D. K. (2013). Principles for valid histopathologic scoring in research. *Veterinary Pathology*, *50*(6), 1007–1015. https://doi.org/10.1177/0300985813485099

Gómez-Barrena, E., Rosset, P., Lozano, D., Stanovici, J., Ermthaller, C., & Gerbhard, F. (2015). Bone fracture healing: Cell therapy in delayed unions and nonunions. *Bone*, *70*, 93–101. https://doi.org/10.1016/j.bone.2014.07.033

Guo, W., Zhang, Y. R., Feng, P., Gao, C. D., Yang, Y. W., Yang, W. J., … Shuai, C. J. (2019). Montmorillonite with unique interlayer space imparted polymer scaffolds with sustained release of Ag+. *Ceramics International*, *45*, 11517–11526.

Han, Z., Bhavsar, M., Leppik, L., Oliveira, K. M., & Barker, J. H. (2018). Histological scoring method to assess bone healing in critical size bone defect models. *Tissue Engineering Part C: Methods*, *24*(5), 272–279. https://doi.org/10.1089/ten.TEC.2017.0497

Kai, D., Prabhakaran, M. P., Chan, B. Q. Y., Liow, S. S., Ramakrishna, S., Xu, F., & Loh, X. J. (2016). Elastic poly (ε-caprolactone)-polydimethylsiloxane copolymer fibers with shape memory effect for bone tissue engineering. *Biomedical Materials*, *11*(1), 015007. https://doi.org/10.1088/1748-6041/11/1/015007

Keramaris, N., Calori, G., Nikolaou, V., Schemitsch, E., & Giannoudis, P. (2008). Fracture vascularity and bone healing: A systematic review of the role of VEGF. *Injury*, *39*, S45–S57.

Khan, M. N., Islam, J. M., & Khan, M. A. (2012). Fabrication and characterization of gelatin-based biocompatible porous composite scaffold for bone tissue engineering. *Journal of Biomedical Materials Research Part A*, *100*(11), 3020–3028.

Knecht, S., Erggelet, C., Endres, M., Sittinger, M., Kaps, C., & Stüssi, E. (2007). Mechanical testing of fixation techniques for scaffold-based tissue-engineered grafts. *Journal of Biomedical Materials Research Part B: Applied Biomaterials*, *83*(1), 50–57.

Marras, S. I., Kladi, K. P., Tsivintzelis, I., Zuburtikudis, I., & Panayiotou, C. (2008). Biodegradable polymer nanocomposites: The role of nanoclays on the thermomechanical characteristics and the electrospun fibrous structure. *Acta Biomaterialia*, *4*(3), 756–765. https://doi.org/10.1016/j.actbio.2007.12.005

Nagasaki, Y. (2011). Construction of a densely poly (ethylene glycol)-chain-tethered surface and its performance. *Polymer Journal*, *43*(12), 949.

Othman, R., Mustafa, Z., Loon, C. W., & Noor, A. F. M. (2016). Effect of calcium precursors and pH on the precipitation of carbonated hydroxyapatite. *Procedia Chemistry*, *19*, 539–545.

Öztürk, A., Yetkin, H., Memis, L., Cila, E., Bolukbasi, S., & Gemalmaz, C. (2006). Demineralized bone matrix and hydroxyapatite/tri-calcium phosphate mixture for bone healing in rats. *International Orthopaedics*, *30*(3), 147–152. https://doi.org/10.1007/s00264-006-0079-x

Panteli, M., Pountos, I., Jones, E., & Giannoudis, P. V. (2015). Biological and molecular profile of fracture non-union tissue: Current insights. *Journal of Cellular and Molecular Medicine*, *19*(4), 685–713. https://doi.org/10.1111/jcmm.12532

Parithimarkalaignan, S., & Padmanabhan, T. (2013). Osseointegration: An update. *The Journal of Indian Prosthodontic Society*, *13*(1), 2–6.

Patel, S., Caldwell, J. M., Doty, S. B., Levine, W. N., Rodeo, S., Soslowsky, L. J., … Lu, H. H. (2018). Integrating soft and hard tissues via interface tissue engineering. *Journal of Orthopaedic Research*, *36*(4), 1069–1077. https://doi.org/10.1002/jor.23810

Pazarçeviren, E., Erdemli, Ö., Keskin, D., & Tezcaner, A. (2017). Clinoptilolite/PCL–PEG–PCL composite scaffolds for bone tissue engineering applications. *Journal of Biomaterials Applications*, *31*(8), 1148–1168. https://doi.org/10.1177/0885328216680152

Polat, E., Karaca, M., Demir, H., & Onus, A. N. (2004). Use of natural zeolite (clinoptilolite) in agriculture. *Journal of fruit and ornamental plant research*, *12*(1), 183–189.

Prabha, R. D., Nair, B. P., Ditzel, N., Kjems, J., Nair, P. D., & Kassem, M. (2019). Strontium functionalized scaffold for bone tissue engineering. *Materials Science & Engineering, C: Materials for Biological Applications*, *94*, 509–515.

Rožić, M., Cerjan-Stefanović, Š., Kurajica, S., Maěefat, M. R., Margeta, K., & Farkaš, A. (2005). Decationization and dealumination of clinoptilolite tuff and ammonium exchange on acid-modified tuff. *Journal of Colloid and Interface Science*, *284*(1), 48–56. https://doi.org/10.1016/j.jcis.2004.09.061

Salmasi, S., Nayyer, L., Seifalian, A. M., & Blunn, G. W. (2016). Nanohydroxyapatite effect on the degradation, osteoconduction and mechanical properties of polymeric bone tissue engineered scaffolds. *The Open Orthopaedics Journal*, *10*, 900–919. https://doi.org/10.2174/1874325001610010900

Stanković, M., Tomar, J., Hiemstra, C., Steendam, R., Frijlink, H. W., & Hinrichs, W. L. J. (2014). Tailored protein release from biodegradable poly(ε-caprolactone-PEG)-b-poly(ε-caprolactone) multiblock-copolymer implants. *European Journal of Pharmaceutics and Biopharmaceutics*, *87*(2), 329–337. https://doi.org/10.1016/j.ejpb.2014.02.012

Sun, M., Chi, G., Li, P., Lv, S., Xu, J., Xu, Z., … Li, Y. (2018). Effects of matrix stiffness on the morphology, adhesion, proliferation and osteogenic differentiation of mesenchymal stem cells. *International Journal of Medical Sciences*, *15*(3), 257.

Thadavirul, N., Pavasant, P., & Supaphol, P. (2014). Development of polycaprolactone porous scaffolds by combining solvent casting, particulate leaching, and polymer leaching techniques for bone tissue engineering. *Journal of Biomedical Materials Research. Part A*, *102*(10), 3379–3392. https://doi.org/10.1002/jbma.35010

Torres, E., Fombuena, V., Valles-Lluch, A., & Ellingham, T. (2017). Improvement of mechanical and biological properties of polycaprolactone loaded with hydroxyapatite and halloysite nanotubes. *Materials Science & Engineering, C: Materials for Biological Applications*, *75*, 418–424.

Türkkan, S., Pazarçeviren, A. E., Keskin, D., Machin, N. E., Duygulu, Ö., & Tezcaner, A. (2017). Nanosized CaP-silk fibroin-PCL-PEG-PCL/PCL based bilayer membranes for guided bone regeneration. *Materials Science and Engineering: C*, *80*, 484–493. https://doi.org/10.1016/j.msec.2017.06.016

Villaca, J. C., da Silva, L., de Alexandria, A. K., de Almeida, G. S., Locatelli, F. R., Maia, L. C., … Cabral, L. M. (2017). Development and characterization of clay-polymer nanocomposite membranes containing sodium alendronate with osteogenic activity. *Applied Clay Science*, *146*, 475–486.

Wang, H., Tong, D., Wang, L., Chen, L., Yu, N., & Li, Z. (2017). A facile strategy for fabricating PCL/PEG block copolymer with excellent enzymatic degradation. *Polymer Degradation and Stability*, *140*, 64–73. https://doi.org/10.1016/j.polymdegradstab.2017.04.015

Zhai, X., Ma, Y., Hou, C., Gao, F., Zhang, Y., Ruan, C., … Liu, W. (2017). 3D-printed high strength bioactive supramolecular polymer/clay nanocomposite hydrogel scaffold for bone regeneration. *ACS Biomaterials Science & Engineering*, *3*(6), 1109–1118. https://doi.org/10.1021/acsbiomaterials.7b00224

SUPPORTING INFORMATION

Additional supporting information may be found online in the Supporting Information section at the end of the article.

Table S1. Histological scoring parameters used for evaluating the degree of healing (Adapted and revised from (Öztürk et al., 2006)).

Table S2. Porosity of scaffolds and total weight loss observed in scaffolds after 28 days of incubation (n = 4).

Table S3. Compressive properties of the scaffolds (n = 4).

How to cite this article: Pazarçeviren AE, Dikmen T, Altunbaş K, et al. Composite clinoptilolite/PCL-PEG-PCL scaffolds for bone regeneration: In vitro and in vivo evaluation. *J Tissue Eng Regen Med*. 2020;14:3–15. https://doi.org/10.1002/term.2938